ORIGINAL ARTICLE   **Open Access**

CrossMark

The effect of pin profiles on the microstructure and mechanical properties of underwater friction stir welded AA2519-T87 aluminium alloy

S. Sree Sabari[*], S. Malarvizhi and V. Balasubramanian

Abstract

Background: AA2519-T87 is a new armour grade aluminium alloy employed in the fabrication of light combat military vehicles. Joining of this material using fusion welding processes, results in the formation of solidification defects like porosity, alloy segregation and hot cracking. In order to overcome the solidification related problems, solid state welding processes such as friction stir welding (FSW) can be used. Though the joining takes place below the melting temperature of the material, the thermal cycle experienced by the thermo-mechanical-affected zone (TMAZ) and heat-affected zone (HAZ) is causing grain coarsening and precipitates dissolution in the age-hardenable aluminium alloys, which deteriorate the joint properties. To get rid of this problem, underwater friction stir welding (UWFSW) process can be employed. The water cooling reduces the heat, and thus, the thermal softening required taking place in TMAZ and HAZ. Therefore, the material flow is entirely different in FSW and UWFSW.

Methods: In this investigation, a comparative study is made to understand the influence of tool pin profiles, namely straight cylindrical (STC), taper cylindrical (TAC), straight threaded cylindrical (THC) and taper threaded cylindrical (TTC) on stir zone characteristics and the resultant tensile properties of both FSW and UWFSW joints.

Results: From this investigation, it is found that the joint made by taper threaded pin profiled tool underwater cooling medium exhibited higher tensile properties of 345 MPa and joint efficiency of 76 %.

Conclusion: The enhancement in the strength is attributed to the precipitation hardening, grain boundary strengthening and narrowing of lower hardness distribution region (LHDR).

Keywords: Friction stir welding, Underwater friction stir welding, Pin profiles, Microstructure, Tensile properties, Microhardness

Background

In recent days, the lighter material is used to construct the light combat vehicles to improve its mobility (Børvik et al. 2011). Among the lighter materials, copper-containing high strength aluminium alloy is the potential candidate which exhibits high toughness and high specific strength to fit into the armour applications. AA2519-T87 is a new generation age-hardenable armour grade aluminium alloy which has good ballistic properties. It is presently well demonstrated that friction stir welding (FSW) process can join aluminium plates with better joint properties over other welding processes (Barcellona et al. 2006; Gachi et al. 2011). The low heat input during FSW avoids the solidification defects and also avoids deteriorated metallurgical transformation that occur at the elevated temperatures (Shukla and Baeslack 2007). Despite, the heat generated during FSW can alter the precipitation behaviour of the aluminium material. The strength and hardness of the age-hardenable aluminium alloys mainly rely on the precipitate type, size and its distribution (Frigaard et al. 2011). During FSW, the thermal condition prevails in the thermo-mechanical-affected zone (TMAZ) and heat-affected zone (HAZ) causes precipitate

* Correspondence: sreesabaridec2006@yahoo.co.in
Centre for Materials Joining and Research (CEMAJOR), Department of Manufacturing Engineering, Annamalai University, Annamalai Nagar, Chidambaram 608 002, Tamil Nadu, India

Sabari *et al. International Journal of Mechanical and Materials Engineering* (2016) 11:5

Page 2 of 14

coarsening and dissolution of precipitates. In addition, the grain coarsening is also occurred in above said zones. Hence, these regions attain lower hardness (softening) and so termed as the lowest hardness distribution region (LHDR) (Fonda and Bingert 2006; Fu et al. 2013).

Zhang et al. studied the microhardness variations in the friction stir welded AA2219 aluminium alloy joint and reported that HAZ recorded lower hardness of 78 HV and hence tensile fracture occurred in this LHDR (Zhang et al. 2011). Similarly, Fonda et al. investigated on the FSW of AA2519 aluminium alloy to study the hardness variations (Fonda and Bingert 2014). Lower hardness values of 80–85 HV were observed in the TMAZ and HAZ, and it was also observed that the tensile fracture occurred in the TMAZ/HAZ interface. In both the above investigations, the hardness values reported in the LHDR were nearly 50 % lower than the hardness of the parent metal. Moreover, they opined that the tensile fracture occurred exactly in the LHDR. Hence, enhancing the hardness of the LHDR is mandatory to improve the joint properties of the FSW joints.

Underwater friction stir welding (UWFSW) is a variant of the FSW process in which the water cooling is utilized to regulate the thermal cycles prevailing in the joint. In FSW process, the joints are fabricated in the air medium (open atmosphere) whereas in UWFSW process, the joints are made in the water medium (submerged in water). During UWFSW, the high heat dissipation capacity of water controls the conduction of heat to TMAZ and HAZ. The low heat prevailing in the TMAZ and HAZ will not be sufficient to coarsen or dissolute the precipitates. In addition, the width of the TMAZ and HAZ can also be minimized by limiting the heat and plastic deformation by UWFSW. Zhang et al. reported that the performance of UWFSW joints of AA2219 Al alloy was enhanced by narrowing the width of the HAZ. Moreover, the controlling of thermal cycles using water cooling improves the hardness from 78 to 98 HV in the LHDR (Zhang et al. 2012). Liu et al. made an investigation on the tensile properties of FSW and UWFSW of AA2219 Al alloy. The study reported that the tensile strength of the UWFSW joint is 5 % higher than the FSW joint (Liu et al. 2010). In an another investigation, Liu et al. reported that the UWFSW AA2219 Al joints showed increase in tensile strength with increase in welding speed, but drastically decreased on further increasing the welding speed and end up with defect formation at the higher welding speed (Liu et al. 2011). Zhang et al. reported that the water cooling improved the tensile strength of FSW AA2219 Al alloy joints at lower welding speed and showed no obvious effect in the higher welding speeds (Zhang et al. 2014).

Though the UWFSW process will yield joints with superior properties, the process parameters and tool geometry has to be selected in such a way to attain defect free, sound joints. The material flow behaviour mainly decides the quality of the FSW joints. The material flow behaviour in FSW depends on the process parameters such as tool rotation speed, tool traverse speed, axial force, tool tilt angle, tool shoulder diameter, tool shoulder profile and tool pin profile. Among the parameters, tool pin profile plays an important role in stirring and extruding the material around the tool pin. The pin profile plays a primary role in controlling the rotary and transverse material flow, though the other parameters are supplementing the material flow by supplying the sufficient heat and force. The flow behaviour of materials in FSW and UWFSW process is entirely different, because of the difference in heat dissipation capacity of the cooling mediums. Hence, the thermal softening in the preheat zone, stir zone and TMAZ differs which in turn causes the difference in material flow behaviour.

Many research works (Chen et al. 2013; Colegrove and Shercliff 2005; Zhao et al. 2014) were previously carried out to understand the flow behaviour of materials in FSW process, but limited research works have been reported so far related to the material flow behaviour of UWFSW process. Hence, in this investigation, an attempt has been made to study the effect of pin profiles on stir zone characteristics and the resultant tensile properties of the joints made by FSW and UWFSW processes.

Methods

Rolled plates of AA2519-T87 aluminium alloy were used as the parent material in this investigation. The chemical composition of the parent metal was quantified using spectro-chemical analysis, and the composition is presented in Table 1. The joint configuration of $150 \times 150 \times 6$ mm was used, and the welding was done normal to the rolling direction using the tools with four different pin profiles, namely straight cylindrical (STC), straight threaded cylindrical (THC), taper cylindrical (TAC) and taper threaded cylindrical (TTC). The dimensions of the four pin profiles are shown in the Fig. 1. The joints were fabricated under air and water cooling mediums, and they are designated as FSW and UWFSW joints, respectively. The process parameters and the welding conditions used to in FSW and UWFSW process are presented in Table 2. These welding parameters were selected based on trial experiments to attain defect free, sound joints. The specimens were extracted from the joints to test and characterize the FSW and UWFSW.

Table 1 Chemical composition (wt%) of AA 2519-T87 aluminium alloy

Cu	Mg	Mn	Fe	V	Si	Ti	Al
5.71	0.47	0.27	0.1	0.05	0.04	0.02	Balance
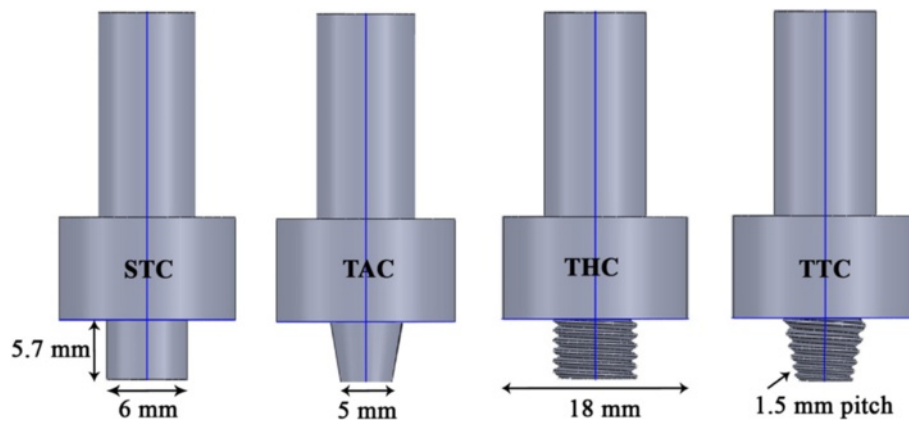
Fig. 1 Dimensions of the tool pin profiles

Metallographic procedures were followed to reveal the microstructural characteristics of the welds by optical microscopy (OM). The OM specimens were polished using water emery papers and etched using Keller's reagent for 10 s to reveal the microstructure. The grain size of stir zone is measured in the pin influenced region (PIR). Similarly, the grain size of TMAZ and HAZ is measured in the mid-thickness region.

One hundred kilo Newton servo controlled universal testing machine (Make: FIE–BLUESTAR, India, Model: UNITEK 94100) was employed to evaluate the transverse tensile properties of the FSW and UWFSW joints. The tensile specimens were extracted, machined and tested as per the ASTM E8M guidelines. Before testing, the samples were flattened to ensure the equal cross-sectional area along the entire gauge length of the specimen. The tensile properties such as yield strength, ultimate tensile strength and elongation were evaluated. The cross section of the tensile tested samples were polished and etched to reveal the entire fracture path using optical microscope. The tensile fracture path was identified by the macro-structural analysis. Scanning electron microscope (SEM) was employed to characterize the fracture surfaces. Hydraulic-controlled

Vickers microhardness tester (Make: Shimadzu and model: HMV-2T) was used to measure the microhardness along the cross section of the weld joint. The indentations were made under the load of 4.9 N for a dwell time of 15 s. The single hardness profile was obtained along the mid-thickness region with the indentation of 1 mm spacing. The correlation between the entire fracture path and the LHDR cannot be agreed from the single hardness profile. Hence, the hardness distribution maps were obtained by indenting along five test lines which are 1 mm spacing along the thickness direction. In each test lines, 25 indentations were made and a total of 125 indentations were made to obtain the hardness distribution map.

Transmission electron microscope (TEM) was employed to characterize the microstructure of the LHDR. Thin sample of 1-mm thick was extracted from the weld joints using wire-cut electro-discharge machining (WEDM) process. The samples were polished to 100-μm thick, and then a 3-mm diameter of sample was extracted from the LHDR for further polishing. The samples were reduced to 10-μm thick using ion milling process to reveal the microstructure under TEM.
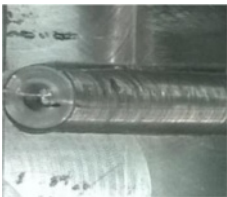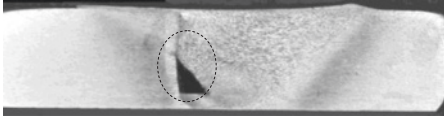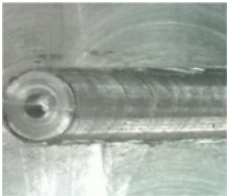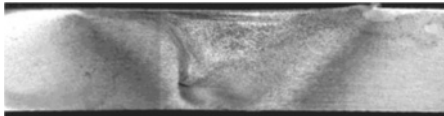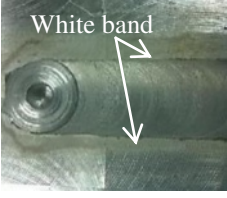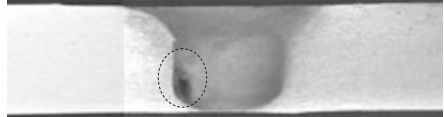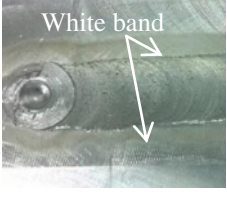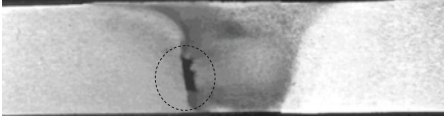
Results
Macrographs
Table 3 shows the appearance of the top surface and the cross-sectional macrograph of the FSW and UWFSW joints fabricated using different pin profiles. The surfaces of all the joints are free from surface defects. The weld surface is smooth and composed of closely spaced ripples in all the joints. However, a distinct band of white region is observed next to the weld region on both sides of the UWFSW joints.
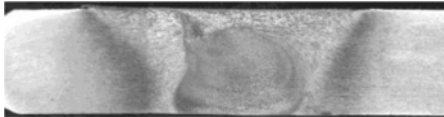
The macro features of the stir zone exhibit different material flow behaviour. From the macrograph, the stir zone can be divided into upper shoulder influenced region (SIR), middle pin influenced region (PIR) and lower

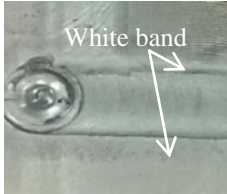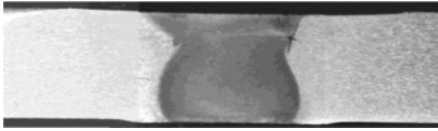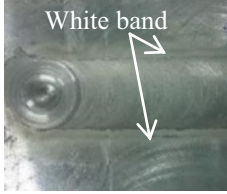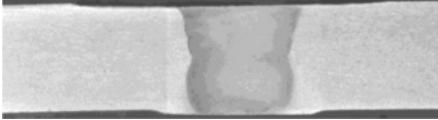**Table 2** Welding parameters and tool dimensions used in this investigation

Process parameters	Values
Tool rotational speed (rpm)	1300
Welding speed (mm/min)	30
Pin length (mm)	5.7
Tool shoulder diameter (mm)	18
Pin diameter (mm)	5–6
Tool tilt angle, degree	2°
Pin profile	Taper threaded pin profile
Tool material	Hardened super high speed steel

Sabari *et al. International Journal of Mechanical and Materials Engineering* (2016) 11:5

Page 4 of 14

Table 3 Effect of tool pin profile on top surface and cross-sectional macrographs

| Name of the joint	Top surface	Cross section	Observation
FSW-STC			Defect-free top surface but tunnel defect is observed at the advancing side
FSW-TAC			Defect-free top surface but tunnel defect is observed at the advancing side
FSW-THC			Defect-free stir zone at both top surface and cross section
FSW-TTC			Defect-free stir zone at both top surface and cross section
UWFSW-STC			Defect-free top surface but tunnel defect is observed at the advancing side
UWFSW-TAC			Defect-free top surface but tunnel defect is observed at the advancing side

Sabari *et al. International Journal of Mechanical and Materials Engineering* (2016) 11:5

Page 5 of 14

Table 3 Effect of tool pin profile on top surface and cross-sectional macrographs *(Continued)*

UWFSW-THC			Defect-free stir zone at both top surface and cross section
UWFSW-TTC			Defect-free stir zone at both top surface and cross section

vortex region (VOR). In both air and water cooling medium, the tunnel defects are observed in the advancing side-PIR of the joints fabricated using STC and TAC profiled tools. But the joints fabricated using THC and TTC profiled tools yielded defect free stir zones in both air and water cooling medium. The defective joints are not considered further analysis, and the defect-free THC and TTC joints alone are considered.

Microstructure

Figure 2 shows the optical micrograph of the parent metal. It is characterized by the presence of elongated grains oriented towards the rolling direction. Figures 3a, b and 4a, b show the stir zone micrographs of the joints fabricated using THC and TTC tools in both air and water cooling medium. It can be observed that dynamic recrystallization has occurred during the FSW and
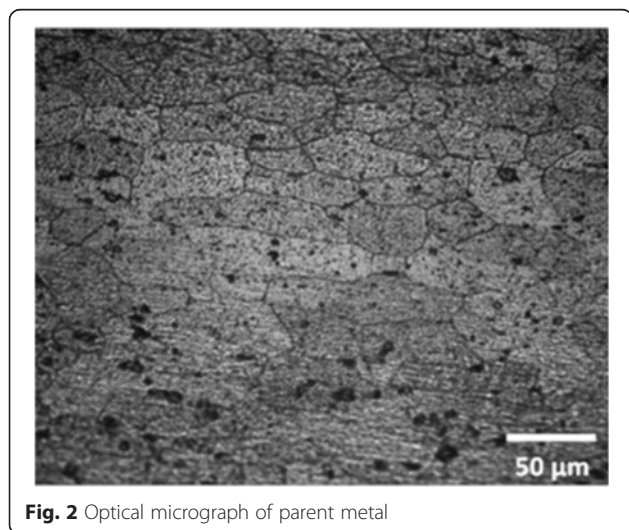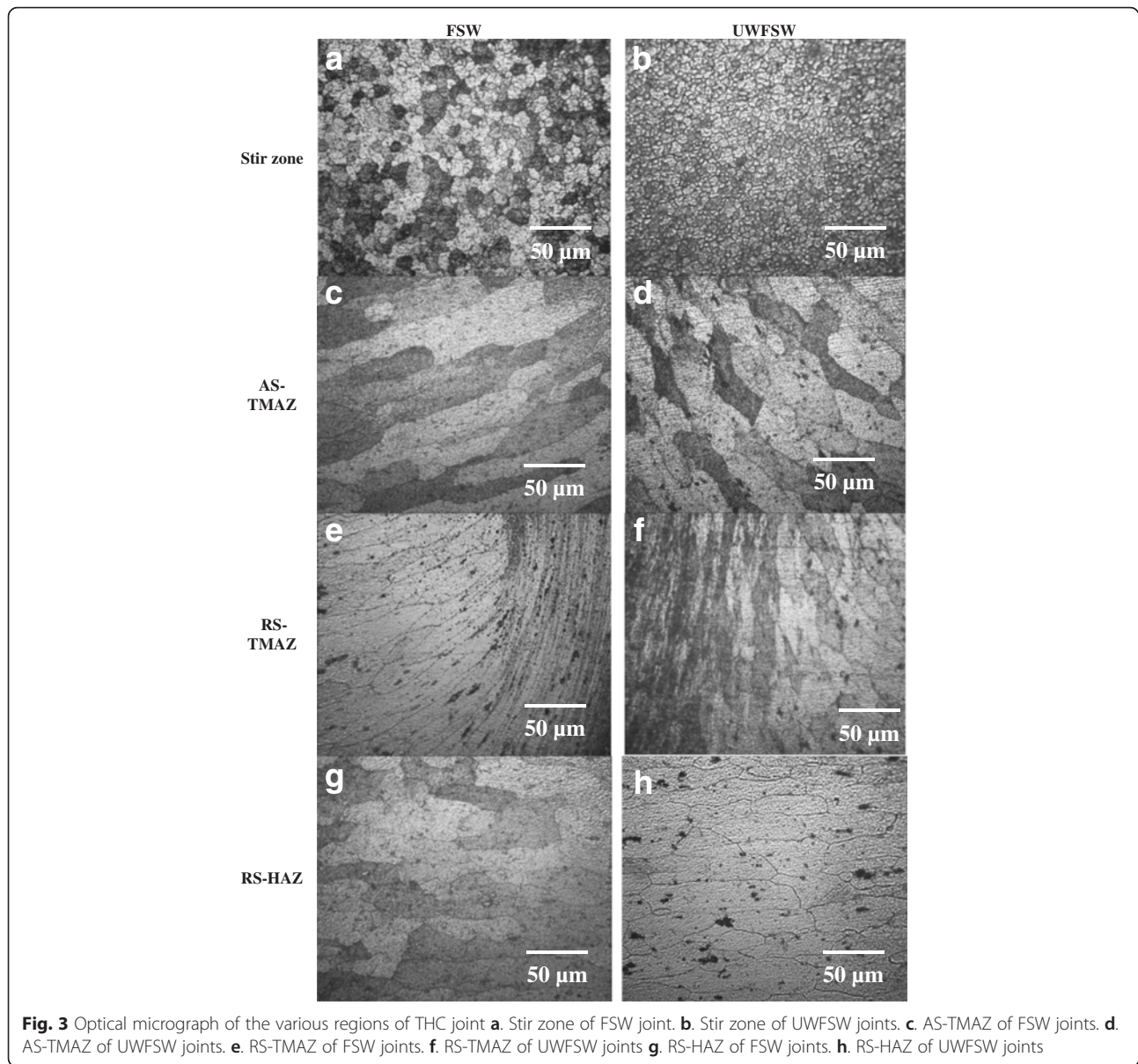

Fig. 2 Optical micrograph of parent metal

UWFSW process. It can also be noticed that grains are fine and equi-axially oriented in the SZ irrespective of the cooling medium. The average grain diameter at various regions were quantified and presented in Table 4. In stir zone, the grain diameter of FSW joints is higher than the UWFSW joints. The joint made using TTC tool shows lower grain size than THC tool under both the cooling mediums and the average grain diameter is 15 and 3.3 μm for FSW and UWFSW joints, respectively. The average grain diameter of the stir zone of the joint made by THC tool is measured as 17.5 and 5.2 μm for FSW and UWFSW joints, respectively.

Figure 3c–f shows the TMAZ micrographs of the joints fabricated using THC in both air and water cooling medium. The advancing side-thermo-mechanically-affected zone (AS-TMAZ) of joint made by THC profiled tool shows coarse and severely deformed elongated grains at the interface. The retreating side-thermo-mechanically-affected zone (RS-TMAZ) micrograph is characterized by elongated and upward oriented grains whereas the deformation is gradually reduced from the interface. Figure 4c–f show the TMAZ micrographs of the joints fabricated using TTC in both air and water cooling medium. The joint fabricated using TTC tool exhibit symmetric material flow in both the AS-TMAZ and RS-TMAZ in both the air cooling and water cooling conditions. The grain size and extent of deformation is more or less similar in both the sides.

The average grain diameter of AS-TMAZ and RS-TMAZ are equal and measured as 54 and 50 μm for the THC and TTC joint, respectively for FSW joints. Similarly, the average grain diameter of AS-TMAZ and RS-TMAZ are equal and measured as 85 and 82 μm for the THC and TTC joint, respectively, for FSW joints. In comparison, the grain diameter of TMAZ of UWFSW joint is
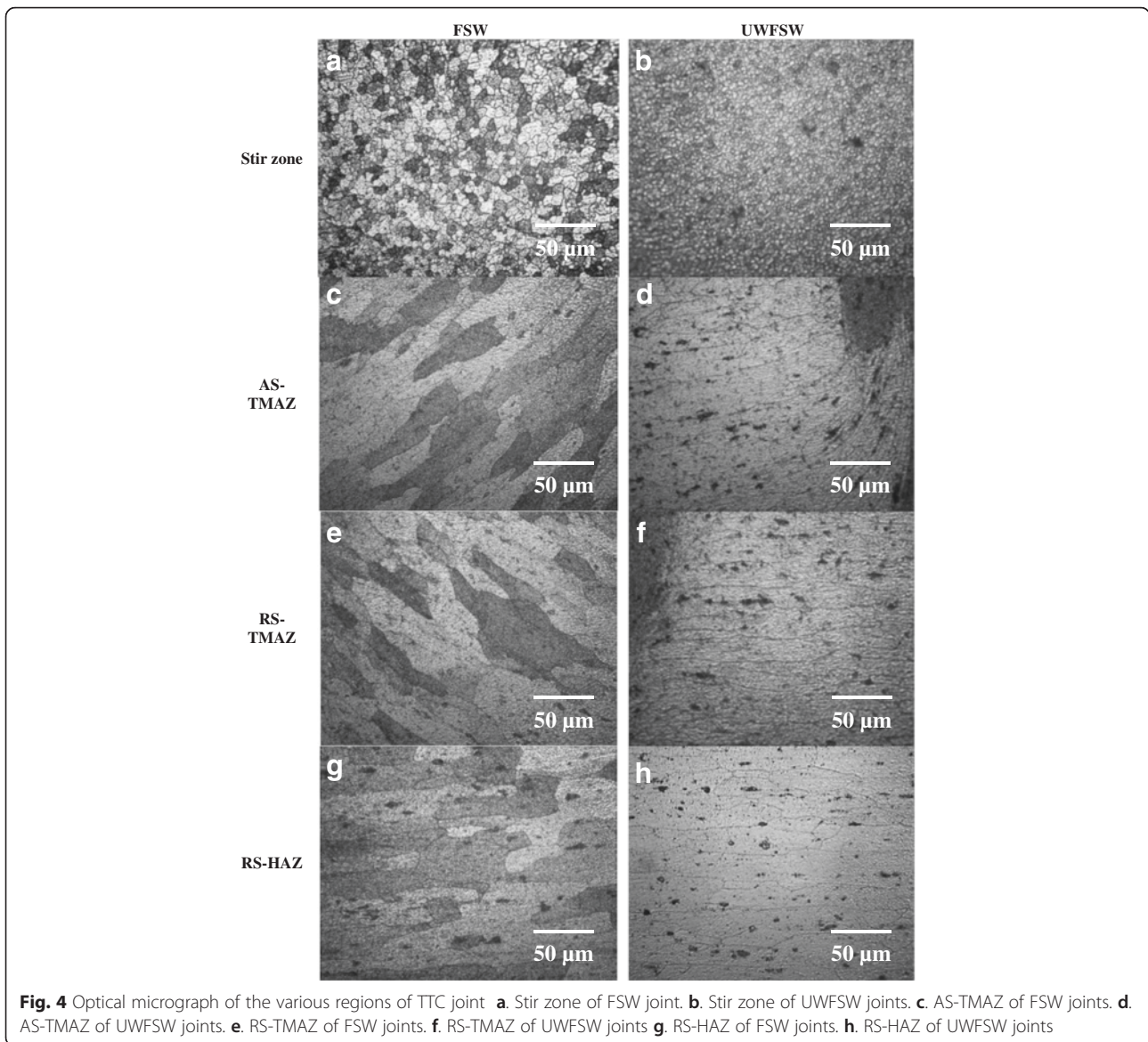
Sabari *et al. International Journal of Mechanical and Materials Engineering* (2016) 11:5

Page 6 of 14

Fig. 3 Optical micrograph of the various regions of THC joint **a**. Stir zone of FSW joint. **b**. Stir zone of UWFSW joints. **c**. AS-TMAZ of FSW joints. **d**. AS-TMAZ of UWFSW joints. **e**. RS-TMAZ of FSW joints. **f**. RS-TMAZ of UWFSW joints **g**. RS-HAZ of FSW joints. **h**. RS-HAZ of UWFSW joints

40 % higher than the FSW joints is respective of pin profiles. It is noticed that the TMAZ micrograph of UWFSW joints shows the interface microstructure from SZ to TMAZ. But at the same magnification level, only a part of TMAZ is seen for the FSW joints. This suggests that the width of the TMAZ region is much wider in FSW joints.

Figures 3g, f and 4g, f show the HAZ micrographs of the joints It is observed that no mechanically induced deformation took place but grain coarsening occurred in all the joints. The HAZ micrograph of the joint made by THC profiled tool reveals larger grains of 52 μm, but TTC joint shows grains of 49 μm in water cooling condition. The HAZ grain size of UWFSW-THC joint is higher than the grain size of PM (of 49 μm) whereas it is equal to the HAZ grain size of UWFSW-TTC joint. In air cooling condition,

the HAZ micrograph of the joint made by THC profiled tool reveals larger size of 64 μm, but TTC joint shows grains of 60 μm. The FSW joints contain coarser grains in HAZ than the UWFSW joints.

Figure 5 shows the TEM micrographs of parent metal and LHDR of all the joints. Figure 5a shows the parent metal micrograph which is characterized by the presence of fine, dense and uniformly distributed θ' ($CuAl_2$) precipitates. The precipitates are oriented in two directions which is normal to each other. The LHDR is characterized by the presence of precipitate free zone (PFZ) and coarsened precipitates. The LHDR of the joints contains lower volume fraction of precipitates than the parent metal. The FSW joints fabricated using THC and TTC profiled pins show more or less identical precipitation behaviour; however, the size of the precipitates of

Sabari *et al. International Journal of Mechanical and Materials Engineering* (2016) 11:5

Page 7 of 14

Fig. 4 Optical micrograph of the various regions of TTC joint **a**. Stir zone of FSW joint. **b**. Stir zone of UWFSW joints. **c**. AS-TMAZ of FSW joints. **d**. AS-TMAZ of UWFSW joints. **e**. RS-TMAZ of FSW joints. **f**. RS-TMAZ of UWFSW joints **g**. RS-HAZ of FSW joints. **h**. RS-HAZ of UWFSW joints
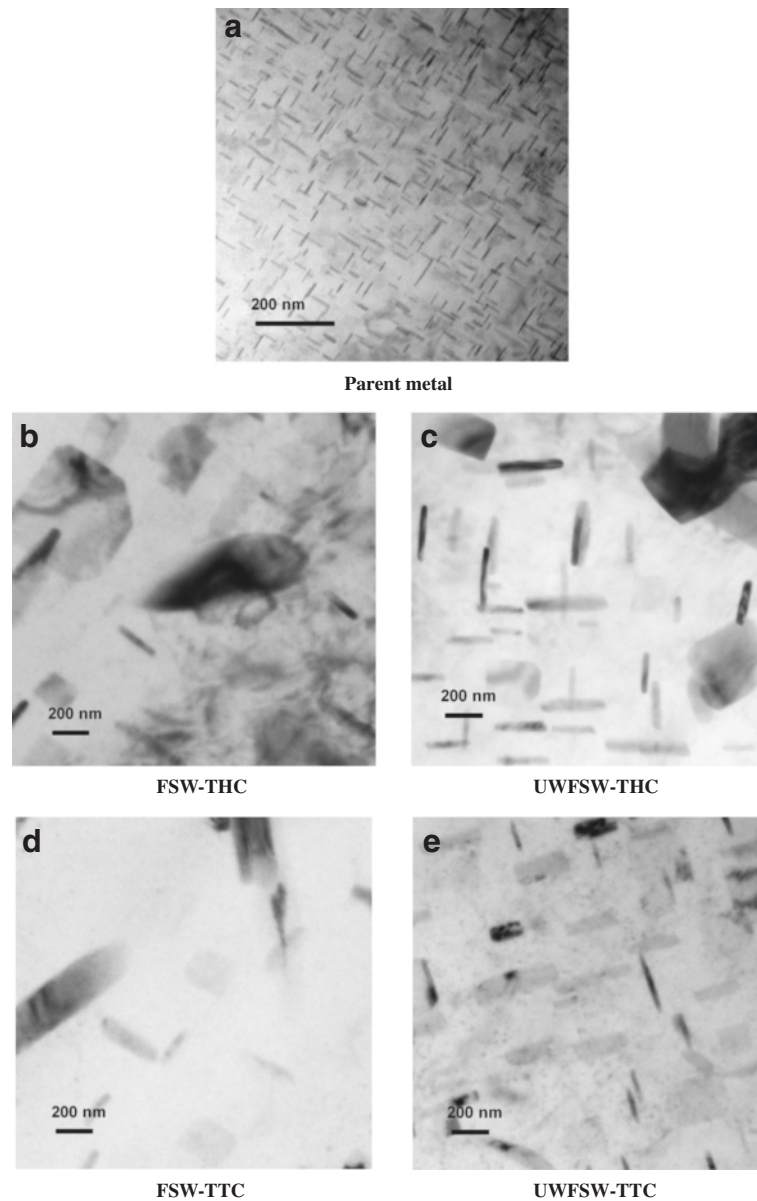
TTC joint is appreciably lower than the THC joints. The LHDR of FSW joints are characterized by the presence of few coarse θ precipitates and larger PFZ. The dissolution of precipitate is relatively lower in LHDR of UWFSW joints, and it is composed of dense coarse stable θ precipitates. From the TEM micrographs, it is evident that the volume fraction of precipitates is higher in UWFSW joints than in FSW joints.

Microhardness

Figure 6 shows the microhardness measurement across the mid-thickness region of the joints. In all the joints, typical W-shaped hardness plots were recorded. Among the various regions, the TMAZ on both the AS and RS of the joints recorded lower hardness. In air cooling condition, FSW-THC joint recorded lowest hardness of 78 HV whereas FSW-TTC joint recorded 80 HV in the RS. In the water

Table 4 Average grain diameter of various regions

Pin profile	SZ (µm)	AS-TMAZ (µm)	RS-TMAZ (µm)	RS-HAZ (µm)	PM (µm)
FSW-THC	17.5	85	85	64	49
FSW-TTC	15	82	82	60	
UWFSW-THC	5.2	54	54	52	
UWFSW-TTC	3.3	50	50	49	

Fig. 5 TEM images of parent metal region and LHDR **a**. Parent metal. **b**. LHDR of FSW-THC. **c**. LHDR of UWFSW-THC. **d**. LHDR of FSW-TTC. **e**. LHDR of UWFSW-TTC

cooling condition, UWFSW-THC joint recorded lowest hardness of 82 HV whereas UWFSW-TTC joint recorded 93 HV in the RS. It is observed that the location of the LHDR is closer to the weld centre in UWFSW joints, but it is marginally away from the weld center in FSW joints. It is also observed that the LHDR is wider in FSW joints and narrower in the UWFSW joints.

In all the joints, the hardness of the SZ are higher than the TMAZ. SZ of UWFSW-TTC joint recorded higher hardness of 105 HV whereas lower hardness of 86 HV was recorded in FSW-THC joint. The hardness of the HAZ are lower; however, it is higher than the TMAZ. It is observed that there is an increase in hardness from TMAZ to PM region. The joint

fabricated using water cooling medium recorded marginally higher hardness in all the regions than the joint fabricated under air cooling medium. Among the pin profiles, the joint fabricated using TTC pin profiled tool in water cooling medium recorded higher hardness than its counterparts.

Tensile properties

Figure 7 shows the stress strain curves of the FSW and UWFSW joints fabricated using THC and TTC tools. The transverse tensile properties like yield strength, ultimate tensile strength and elongation are derived from the stress strain curves and presented in the Table 5. The unwelded parent metal (PM) showed
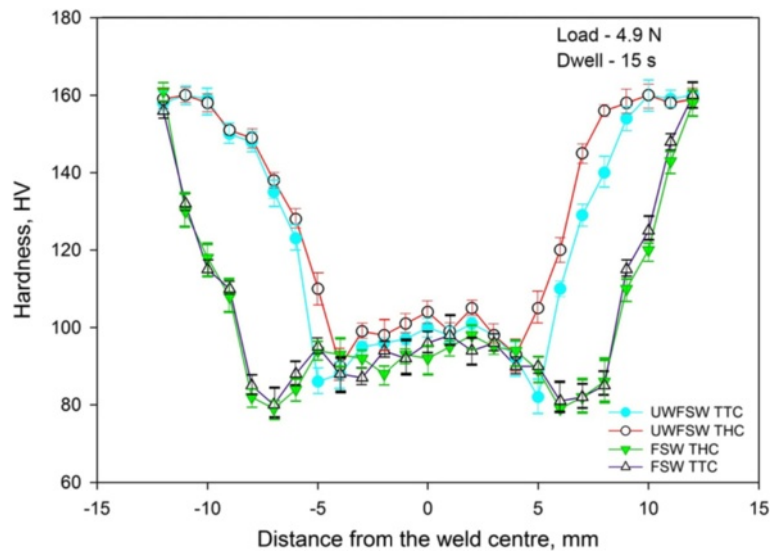
Sabari *et al. International Journal of Mechanical and Materials Engineering* (2016) 11:5

Page 9 of 14

Fig. 6 Microhardness plot

tensile strength of 452 MPa with an elongation of 11.2 %. The UWFSW-THC joint exhibited tensile strength of 327 MPa which is 30 % lower than PM, and it showed an elongation of 7.94 % which is also 30 % lower than PM. The UWFSW-TTC joint yielded tensile strength of 345 MPa which is 25 % lower than PM, and it showed an elongation of 9.17 % which is 20 % lower than PM. FSW-TTC joint exhibited tensile strength of 267 MPa and joint efficiency of 59 % which is 9 % higher than the FSW-THC joint. Of the four joints, UWFSW-TTC joint showed higher joint

efficiency of 76 % which is 5 % higher than UWFSW-THC joint, 29 % higher than FSW-THC joint and 22 % higher than FSW-TTC joint.

Fracture surface

Table 6 shows the fracture location of the tensile tested specimen. The cross-sectional macrograph of the fractured specimen reveals the entire fracture path. It can be clearly seen that the fracture is observed in the TMAZ in all the joints. The FSW joints show the regular fracture path which is 45°
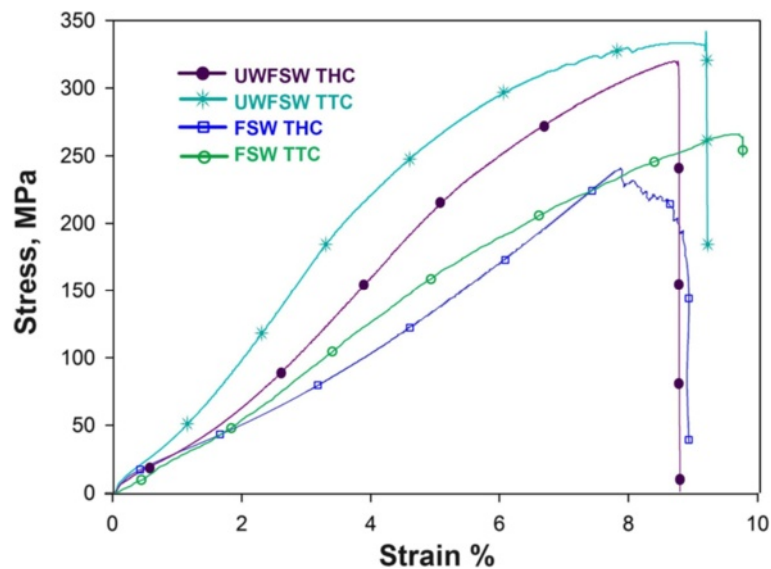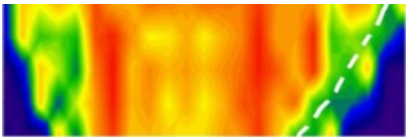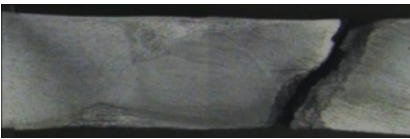

Fig. 7 Stress strain curves

Sabari *et al. International Journal of Mechanical and Materials Engineering* (2016) 11:5

Page 10 of 14
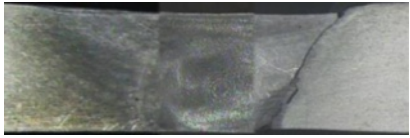
Table 5 Transverse tensile properties of the joints

	0.2 % Yield strength (MPa)	Tensile strength (MPa)	Elongation in 50-mm gauge length (%)	Joint efficiency (%)
Parent metal	427	452	11.2	–
UWFSW-THC	301	327	7.94	72
UWFSW-TTC	322	345	9.17	76
FSW-THC	218	244	9.2	54
FSW-TTC	230	267	9.85	59

inclined to the tensile loading direction. But the UWFSW joints show an irregular fracture path along the outer periphery of the stir zone. From the hardness map, it is yet again confirmed that the LHD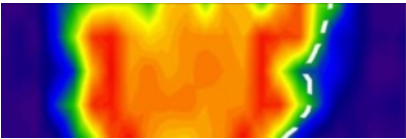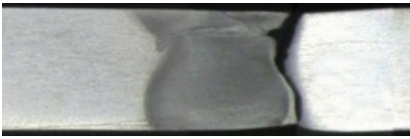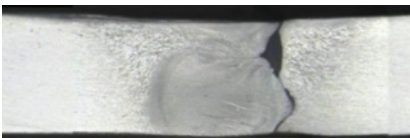R is present at both the AS and RS. The dotted lines imposed on the hardness map describe fracture location and the fracture path. The fracture path is having close agreement with the LHDR of the hardness maps of all the joints.

Figure 8 shows the typical fracture surface at macro- and microlevel magnifications. The joints fabricated using THC and TTC pin profile in water cooling medium shows two different patterns on fracture surface, one at the SIR and another at PIR. But the entire fracture region of FSW-THC and FSW-TTC joints exhibit only one fracture pattern. At higher magnification, all the joints show fine populated dimples in the fracture surface, irrespective of the pin profiles and cooling

Table 6 Effect of tool pin profile on fracture path

Name of the joint	Micrograph map	Fracture path	Observation
FSW-THC			Fracture is occurred in the RS-TMAZ which is 45° inclined to the loading direction
FSW-TTC			Fracture is occurred in the RS-TMAZ which is 45° inclined to the loading direction
UWFSW-THC			Fracture is occurred in the TMAZ in which the fracture is irregular
UWFSW-TTC			Fracture is occurred in the TMAZ in which the fracture is irregular

78 90 100 110 120 130 140 150 160

Fig. 8 Fracture analysis
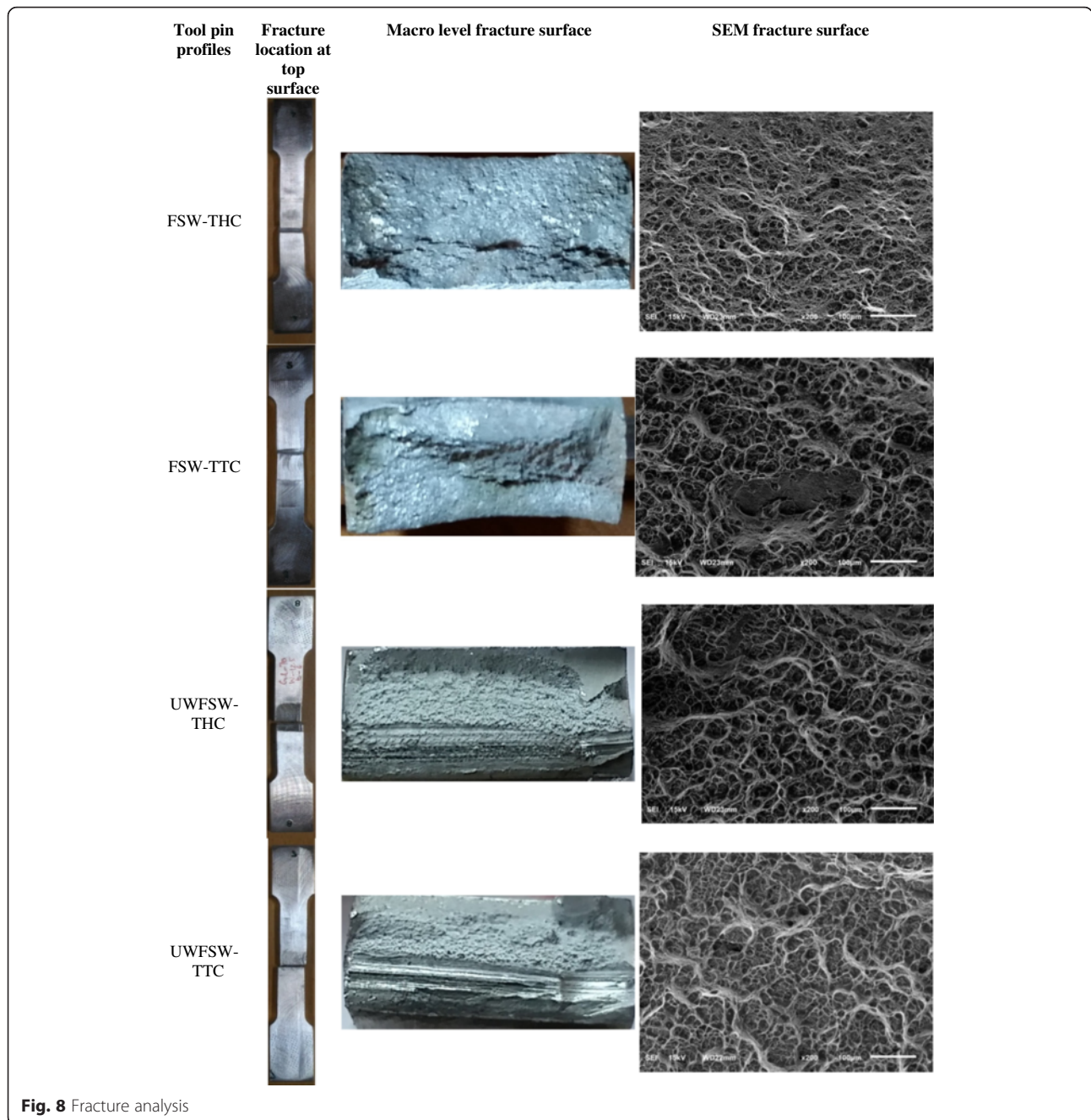
medium. The dimples are oriented towards the loading direction and the presence of dimples suggests that the joints are failed predominantly in the ductile mode.

Discussion

The effect of tool pin profiles on the joint quality

In UWFSW process, the soundness of joint is decided by the heat generation and the material flow behaviour (Mishra & Ma 2005). The heat generation and material flow are classified into three states, namely insufficient state, balance state and excess state. The tool pin profile is one of the predominant parameters controlling these states. The defect-free joints can be made, if the proper tool pin profile is used for making FSW joints (Suresha et al. 2011; Zhao et al. 2005; Kumar et al. 2011).

In this investigation, the defect-free joints were achieved while using THC and TTC pin profiled tools in both air and water cooling medium. During each rotation of the tool, the threaded profile extrudes cylindrical sheets of material around the tool pin from AS to RS and from RS to AS. The peaks and valleys of threaded

Sabari *et al. International Journal of Mechanical and Materials Engineering* (2016) 11:5

Page 12 of 14

pin profile offer more friction over the plasticized material which promotes sticking condition. Thus, the extent of heat generation and plasticization is sufficient to attain the balance state of heat and material flow. In general, the defect is formed in the weld periphery, i.e. the transformed layers around the tool pin. So, the pin profile should capable of forming sufficient transforming layers. By creating enough transforming layers by plasticization and shearing of materials, the threaded pin profiles (THC and TTC) are capable of resulting sound joints.

The joints fabricated using STC and TAC pin profile, using both cooling medium, resulted in defects at the stir zone. The plain, featureless surface area offers lower friction over the plasticized material which promotes slipping condition. In addition, the featureless surface cannot direct the material flow intensively. Palanivel et al. reported that the plain taper surface results drop in frictional heat because of lower heat generation during sliding over sticking condition (Palanivel et al. 2012). Thus, an insufficient heat state is prevailing in the SZ while using the above two pin profiles.

The STC pin profile is plain and straight, and thus, it exhibits a regular material flow during welding. The material transport from AS to RS and from RS to AS is uniform from SIR to PIR, i.e. top to bottom of the joint. Usually, it is not preferable because the heat generation is varied from SIR to PIR. Thus, the optimum combination of heat input and material flow is not met throughout the stir zone. The material flow should vary as like heat input to attain the balance state of heat and material flow. The size of the defect is larger in air cooling condition than the water cooling condition. The size of the defect should be reduced as approaching from insufficient heat state to balance state. Thus, it is inferred that the STC pin profile cannot create defect-free stir zone, since the plain and straight profile cannot able to support and direct the material to flow. Thus, in STC joints, the defects are formed primarily due to the attainment of insufficient material flow state rather due to the heat state.

In TAC pin profile, the tapers are beneficial for aiding upwards and downward flow; however, the plain, featureless surface area creates lower friction which promotes slipping condition. In underwater condition, the heat generated is low, and thus, insufficient heat state is attained. But, during the air cooling condition, the heat generated is high and it is approaching the balance heat state. As the heat generated increases, the size of the defect is decreased. Thus, in TAC joints, the defects are formed due to the insufficient heat and material flow state.

Because of the insufficient heat generation and poor material flow, the plastic deformation around the pin is limited, and thus, the formation of transforming layer is limited. Thus, the joints fabricated using STC and TAC tool exhibited defects in the stir zone. The wider transforming layer created around the tool pin with the help of threads is the prime reason for the defect-free stir zone formation. By this way, the threaded pin profile tools create the balance state of heat and material flow to form the defect-free stir zone.

It is also inferred that the change of cooling medium does not significantly influence the mechanism of defect formation. This is because the FSW process is carried out by localize application of frictional heat and pressure. The heat and pressure experienced is almost similar in FSW and UWFSW joints. The effect of cooling is higher in the TMAZ and HAZ region and minimal in the SZ. However, the extent of heat loss from SZ is different which varies the defect size, grain size and resultant mechanical properties.

The effect of tool pin profiles on microstructure

The heat generation and the plastic deformation during FSW and UWFSW process drive the recrystallization process in the stir zone (Liu et al. 2010; Zhang et al. 2014). Thus, a new set of fine grains are observed in the stir zones of the joints fabricated using THC and TTC tools in both the cooling conditions. In the TMAZ, the heat input and the deformation is not sufficient to recrystallize the grains (Yoon et al. 2015). Thus, elongated coarse grains are observed in both the joints. The HAZ only experiences the heat and no deformation is occurred; hence, this region exhibit undeformed coarse grains. The high heat dissipation capacity of water, readily convect the heat from the SZ, TMAZ and HAZ. Thus, the heat availability in UWFSW in various regions is lower than the FSW joints. During the FSW process, the loss of heat due to air cooling is minimal. Because of high heat input and slow cooling rate, the joint fabricated using air cooling medium reveals marginally larger grains and wider stir zone than the joint fabricated using water cooling medium. In FSW joint, the width of TMAZ is wider and it is located away from the weld centerline. This is attributed to the presence of wider stir zone and occurrence of extensive deformation in the TMAZ. In addition to the change of the cooling medium, the change of pin profile has effect in heat generation. The THC profiled tool exhibit larger frictional contact area to create higher frictional heat than TTC profiled tool pin. Thus, the THC joint exhibit high heat input and slow cooling rate than the TTC joint.

Zhang et al. (Fu et al. 2013) referred SZ as the reprecipitation zone, SZ-TMAZ interface as the dissolution zone and TMAZ to HAZ as the overaging zone. During FSW and UWFSW process, the heat generated is high to solutionize the precipitates in the SZ. On cooling cycle,

Sabari *et al. International Journal of Mechanical and Materials Engineering* (2016) 11:5

Page 13 of 14

the heat is utilized to reprecipitate in the SZ. In the SZ-TMAZ interface, the heat is sufficient to solutionize the precipitates, but unable to reprecipitate because of the high cooling rate. The heat prevails in the regions from TMAZ to HAZ is not sufficient to solutionize and so coarsening of precipitate is happening in the above said regions. Thus, these regions are termed as overaged zone. Because of this reason, TMAZ undergone overaging during FSW and UWFSW and coarse precipitates are observed. However, both coarsening and the dissolution of precipitates are observed in the LHDR because of the heterogeneous precipitation. Increase in heat input increases the precipitate size and dissolution of precipitates. Hence, the high input FSW-THC joint exhibits low volume fraction of coarse precipitates in the LHDR.

The effect of tool pin profiles on the mechanical properties of the joints

The age-hardenable materials are mainly strengthened due to the presence of fine θ' precipitates. During loading, these precipitates act as the obstacle for the dislocation motion. The coarse stable θ precipitates cannot provide the hindrance effect due to low coherency. From the Hall-Petch relation, it was understood that the hardness or strength decreases with an increase in the grain size (Xu et al. 2012). The TMAZ micrographs exhibit coarser grains and so reduced grain boundary strengthening is observed in this region. Thus, the lower hardness of LHDR is attributed to the low grain boundary strengthening and precipitate hardening.

The heat input governs the above said strengthening mechanism. Decrease in heat input will increase the strengthening effects. Thus, the UWFSW joint recorded higher hardness in the entire region than the FSW joint and therefor the UWFSW joint exhibited higher tensile strength than the FSW joint. The higher tensile strength is attributed to the presence of relatively fine grains, high volume fraction of precipitates and appreciably narrow LHDR. On comparing the four joint conditions (FSW-THC, FSW-TTC, UWFSW-THC and UWFSW-TTC), the UWFSW-TTC joint shows enhanced tensile and hardness properties because this joint experience the lowest temperature compared to its counterparts. So, the pin profile capable of formation of the defect-free stir zone at the minimum heat input is appreciable.

During tensile loading, the load will concentrate on the weakest zone in the joint. The TMAZ is identified as the LHDR, and thus, the load is concentrated on it and the failure occurred in this region. This is consistent with the microhardness map and the fracture locations of both the joints (Table 6). Thus, the fracture is occurring in the weakest region, i.e. at TMAZ. The FSW joints exhibit wider LHDR, and the UWFSW joints exhibit narrow LHDR near to the weld periphery. Because of wider LHDR, the fracture path is 45° to the loading direction and the failure is occurred by simple shearing. But in UWFSW joints, due to narrowed LHDR, the fracture path is restricted near to the weld periphery, and thus, the shape of the fracture path is similar to the shape of the weld periphery. In addition, the grain orientation difference at the interface offers resistance to the tensile fracture, and thus, the fracture surface is not smooth.

From the tensile test results, it was observed that the weld joint undergone reduction in the ductility property (Table 5). The measures of ductility, i.e. elongation of the joints were lower than the parent metal. The poor precipitation strengthening and grain boundary strengthening of TMAZ offers less resistance to tensile load. Therefore, the load was accommodated in TMAZ which cause yielding of TMAZ. The load concentration phenomenon is called strain localization (Fu et al. 2011). Because of strain localization, the TMAZ alone contributes to elongate during tensile loading. Therefore, a reduced elongation value was observed in the joints compare to the parent metal. The elongation of joints are almost similar; however, the UWFSW joints exhibit lower elongation than the FSW joints. This was attributed to the narrow TMAZ of UWFSW joints which undergone high extent of strain localization than the FSW joints.

Conclusions

The effect of tool pin profiles on the stir zone characteristics and tensile properties of friction stir welded and underwater friction stir welded AA2519-T87 aluminium alloy joints were investigated and the following conclusions are derived:

1) Of the four tool pin profiles used in this investigation, straight threaded cylindrical (THC) pin profile and taper threaded cylindrical (TTC) pin profile yielded defect-free weld surface and stir zone formation in both air cooling and water cooling medium. It is attributed to the attainment of balance state of heat generation and material flow during stirring.
2) The UWFSW-TTC joint fabricated using taper threaded pin profile with water cooling exhibited tensile strength of 345 MPa and joint efficiency of 76 %, which is 5 % higher than UWFSW-THC joint, 29 % higher than FSW-THC joint and 22 % higher than FSW-TTC joint.
3) The presence of relatively finer grains in the stir zone, higher volume fraction of precipitates, marginally higher hardness of stir zone and appreciably lower width of lower hardness distribution region are the main reasons for the better performance of UWFSW-TTC joints than its counterparts.

Sabari *et al. International Journal of Mechanical and Materials Engineering* (2016) 11:5

Page 14 of 14

References

Barcellona, A, Buffa, G, Fratini, L, & Palmeri, D. (2006). On microstructural phenomena occurring in friction stir welding of aluminium alloys. *Journal of Materials Processing Technology, 177*, 340–343.

Børvik, T, Olovsson, L, Dey, S, & Langseth, M. (2011). Normal and oblique impact of small arms bullets on AA6082-T4 aluminium protective plates. *International Journal of Impact Engineering, 38*, 577–589.

Chen, G, Shi, Q, Li, Y, Sun, Y, Dai, Q, Jia, J, Zhu, Y, & Wu, J. (2013). Computational fluid dynamics studies on heat generation during friction stir welding of aluminum alloy. *Computational Materials Science, 79*, 540–546.

Colegrove, PA, & Shercliff, HR. (2005). 3-Dimensional CFD modelling of flow round a threaded friction stir welding tool profile. *Journal of Materials Processing Technology, 169*, 320–327.

Fonda, RW, & Bingert, JF. (2006). Precipitation and grain refinement in a 2195 Al friction stir weld. *Metallurgical and Materials Transactions A, 37*(12), 3593–3604.

Fonda, RW, & Bingert, JF. (2014). Microstructural evolution in the heat-affected zone of a friction stir weld. *Metallurgical and Materials Transactions A, 35A*, 1487–1499.

Frigaard, Ø, Grong, Ø, & Midling, OT. (2011). A process model for friction stir welding of age hardening aluminum alloys. *Metallurgical and Materials Transactions A, 32A*, 1189–1200.

Fu, R, Sun, Z, Sun, R, Li, Y, Liu, H, & Liu, L. (2011). Improvement of weld temperature distribution and mechanical properties of 7050 aluminum alloy butt joints by submerged friction stir welding. *Materials and Design, 32*, 4825–4831.

Fu, R, Zhang, J, Li, Y, Kang, J, Liu, H, & Zhang, F. (2013). Effect of welding heat input and post-welding natural aging on hardness of stir zone for friction stir-welded 2024-T3 aluminum alloy thin-sheet. *Materials Science and Engineering A, 559*, 319–324.

Gachi, S, Boubenider, F, & Belahcene, F. (2011). Residual stress, microstructure and microhardness measurements in AA7075-T6 FSW welded sheets. *Nondestructive of Testing and Evaluation, 26*, 1–11.

Kumar, K, Satish Kailas, V, & Srivatsan, TS. (2011). The role of tool design in influencing the mechanism for the formation of friction stir welds in aluminum alloy 7020. *Materials and Manufacturing Processes, 26*, 915–921.

Liu, HJ, Zhang, HJ, Huang, YX, & Yu, L. (2010). Mechanical properties of underwater friction stir welded 2219 aluminum alloy. *Transactions of the Nonferrous Metals Society of China, 20*, 1387–1391.

Liu, HJ, Zhang, HJ, & Yu, L. (2011). Effect of welding speed on microstructures and mechanical properties of underwater friction stir welded 2219 aluminum alloy. *Materials and Design, 32*, 1548–1553.

Mishra, RS, & Ma, ZY. (2005). Friction stir welding and processing. *Materials Science and Engineering R, 50*, 1–78.

Palanivel, R, Koshy Mathews, P, Murugan, N, & Dinaharan, I. (2012). Effect of tool rotational speed and pin profile on microstructure and tensile strength of dissimilar friction stir welded AA5083-H111 and AA6351-T6 aluminum alloys. *Materials and Design, 40*, 7–16.

Shukla, AX, & Baeslack, WA. (2007). Study of microstructural evolution in friction-stir welded thin-sheet Al–Cu–Li alloy using transmission-electron microscopy. *Scripta Materialia, 56*, 513–516.

Suresha, CN, Rajaprakash, BM, & Upadhya, S. (2011). A study of the effect of tool pin profiles on tensile strength of welded joints produced using friction stir welding process. *Materials and Manufacturing Processes, 26*, 1111–1116.

Xu, WF, Liu, JH, Chen, DL, Luan, GH, & Yao, JS. (2012). Improvements of strength and ductility in aluminum alloy joints via rapid cooling during friction stir welding. *Materials Science and Engineering A, 548*, 89–98.

Yoon, S, Ueji, R, & Fuji, H. (2015). Effect of rotation rate on microstructure and texture evolution during friction stir welding of Ti-6Al-4V plates. *Materials Science and Engineering, 10*, 103–107.

Zhang, HJ, Liu, HJ, & Yu, L. (2011). Microstructure and mechanical properties as a function of rotation speed in underwater friction stir welded aluminum alloy joints. *Materials and Design, 32*, 4402–4407.

Zhang, HJ, Liu, HJ, & Yu, L. (2012). Effect of water cooling on the performances of friction stir welding heat-affected zone. *Journal of Materials Engineering and Performance, 21*, 1182–1187.

Zhang, Z, Xiao, BL, & Ma, ZY. (2014). Influence of water cooling on microstructure and mechanical properties of friction stir welded 2014Al-T6 joints. *Materials Science and Engineering A, 614*, 6–15.

Zhao, Y, Lin, S, Wu, L, & Qu, F. (2005). The influence of pin geometry on bonding and mechanical properties in friction stir weld 2014 Al alloy. *Materials Letters, 59*, 2948–2952.

Zhao, Y, Wang, Q, Chen, H, & Yan, K. (2014). Microstructure and mechanical properties of spray formed 7055 aluminum alloy by underwater friction stir welding. *Materials and Design, 56*, 725–730.